Title

Ultralow-loss polaritons in isotopically pure boron nitride

Journal

Nature Materials, 17(2)

ISSN

1476-1122

Authors

Giles, Alexander J

Dai, Siyuan

Vurgaftman, Igor

et al.

Publication Date

2018-02-01

DOI

10.1038/nmat5047

Peer reviewed

LETTERS
PUBLISHED ONLINE: 11 DECEMBER 2017 | DOI: 10.1038/NMAT5047
nature materials

Ultralow-loss polaritons in isotopically pure boron nitride

Alexander J. Giles[1]*, Siyuan Dai[2], Igor Vurgaftman[1], Timothy Hoffman[3], Song Liu[3], Lucas Lindsay[4], Chase T. Ellis[1], Nathanael Assefa[5], Ioannis Chatzakis[6], Thomas L. Reinecke[1], Joseph G. Tischler[1], Michael M. Fogler[2], J. H. Edgar[3], D. N. Basov[2,7] and Joshua D. Caldwell[8]

Conventional optical components are limited to size scales much larger than the wavelength of light, as changes to the amplitude, phase and polarization of the electromagnetic fields are accrued gradually along an optical path. However, advances in nanophotonics have produced ultrathin, so-called 'flat' optical components that beget abrupt changes in these properties over distances significantly shorter than the free-space wavelength[1–8]. Although high optical losses still plague many approaches[9], phonon polariton (PhP) materials have demonstrated long lifetimes for sub-diffractional modes[10–13] in comparison to plasmon-polariton-based nanophotonics. We experimentally observe a threefold improvement in polariton lifetime through isotopic enrichment of hexagonal boron nitride (hBN). Commensurate increases in the polariton propagation length are demonstrated via direct imaging of polaritonic standing waves by means of infrared nano-optics. Our results provide the foundation for a materials-growth-directed approach aimed at realizing the loss control necessary for the development of PhP-based nanophotonic devices.

Due to the long free-space wavelengths in the infrared to terahertz spectral domain, the realization of flat and sub-diffractional-scale optical components promises tremendous advances in imaging, communications, integrated photonics and waveguides. Truly nanoscale photonic elements in the infrared require the use of polaritons—quasiparticles composed of an oscillating charge and a photon—that enable the confinement of light to size scales well below the diffraction limit[14,15]. In this spectral range, the oscillating charge arises from either free carriers within metals and doped-semiconductors (plasmon polaritons, PPs), or ionic charges on a polar crystal lattice (phonon polaritons, PhPs)[11]. Generating these polaritons occurs within materials exhibiting a negative real part of the dielectric function, $\mathrm{Re}(\varepsilon) < 0$, which occurs at frequencies below the plasma frequency for PPs or between the transverse (TO) and longitudinal (LO) optical phonons (the Reststrahlen band) for PhPs. As optical phonons exhibit much longer lifetimes than free carriers, the optical losses of PhPs are significantly lower than their PP counterparts. This has been experimentally demonstrated by the very large quality factors reported for sub-diffraction optical antennas[11–13,16]. That said, the fast dispersion of the dielectric function within the Reststrahlen band also results in slow group velocities for the PhP modes and thus limits the propagation length[10,17]. Isotopically pure materials, extensively investigated by Cardona and others[18,19], have phonon frequencies shifted and linewidths narrowed compared to materials with mixtures of isotopes[18]. Thus, using such isotopically pure materials, we demonstrate significant enhancement in PhP propagation, enabling substantial improvements in waveguides and hyperlenses, among other potential applications[6,20–22].

Hexagonal boron nitride (hBN) is a polar dielectric material that is particularly well suited for nanophotonic components[6,12,17,20,23–25]. As a two-dimensional van der Waals crystal, hBN exhibits an extremely large crystalline anisotropy resulting from strong, in-plane covalent bonding of boron and nitrogen atoms and weak, out-of-plane, interlayer van der Waals bonding. This gives rise to two spectrally distinct bands where PhPs can be supported, designated as the lower (LR, $\sim$760–820 cm^{-1}) and upper (UR, $\sim$1,365–1,610 cm^{-1}) Reststrahlen bands[12,24]. Further, the strong anisotropy results in a large birefringence, where within the Reststrahlen bands, the dielectric permittivities along orthogonal crystal axes are not only different, but opposite in sign. Such materials are referred to as hyperbolic[26]. In the case of hBN, the in-plane permittivity is isotropic and is defined with a single value, ε_t, which is negative (positive) in the UR (LR), whereas the out-of-plane component ε_z is positive (negative). Previous results have shown that the long optical phonon lifetimes enabled quality factors in (naturally abundant) hBN nanostructures that are well in excess of the highest reported values in PP-based systems[12,25].

The most common type of point defect responsible for optical phonon scattering in hBN is the natural isotope variation of boron: $\sim$80% ^{11}B and $\sim$20% ^{10}B (^{14}N is 99.6% abundant). Thus, a change of only one atomic mass unit represents a $\sim$10% change in the boron mass. Therefore, one could anticipate that large increases in phonon lifetimes could be realized through isotopic enrichment. Through the use of isotopically enriched boron powder as one of the precursors, hBN crystals with isotope purities as high as $^{11}\mathrm{B} = 99.2\%$ and $^{10}\mathrm{B} = 98.7\%$ were grown from molten metal solutions (see Methods)[27,28]. The absolute ratio of the two boron isotopes was quantified using secondary ion mass spectrometry (SIMS) for several samples of different isotopic enrichments, including all samples discussed here. Through comparison of the SIMS-determined ratios with the in-plane E_{2g} phonon energies extracted from Raman spectroscopy, a relationship was established, allowing the isotopic ratio to be approximated via the Raman shift (see Supplementary Information). Further, an estimate of the

[1]United States Naval Research Laboratory, Washington DC 20375, USA. [2]Department of Physics, University of California San Diego, San Diego, La Jolla, California 92093, USA. [3]Department of Chemical Engineering, Kansas State University, Manhattan, Kansas 66506, USA. [4]Materials Science and Technology Division, Oak Ridge National Laboratory, Oak Ridge, Tennessee 37830, USA. [5]NREIP Summer Student residing at NRL, Washington DC 20375, USA. [6]ASEE Postdoctoral Fellow residing at NRL, Washington DC 20375, USA. [7]Department of Physics, Columbia University, New York, New York 10027, USA. [8]Vanderbilt University, Nashville, Tennessee 37235, USA. *e-mail: alexander.giles@nrl.navy.mil

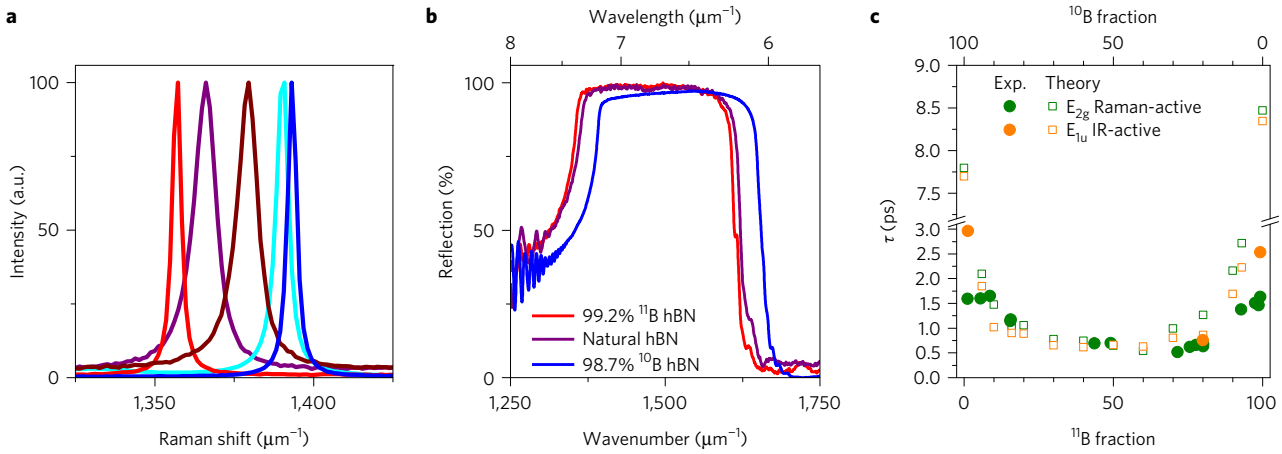

Figure 1 | Influence of isotopic enrichment on hBN optic phonons. a, 532 nm Raman spectra of the E_{2g} mode from hBN crystals with a variety of isotopic enrichments (red—^{10}B 98.7%, purple—natural abundant, brown—^{10}B 51%, cyan—^{11}B 83% and blue—^{11}B 99.2%). A clear reduction in linewidth and spectral shift of the E_{2g} phonon is observed with the enriched samples. **b**, FTIR reflection spectra of hBN crystals with high isotopic purity in comparison to a crystal with the naturally abundant ^{10}B:^{11}B ratio of ~20%:80%. **c**, E_{2g} (green open squares) and E_{1u} (orange open squares) phonon lifetimes for hBN calculated as a function of ^{11}B enrichment. E_{2g} and E_{1u} phonon lifetimes determined from the Raman measurements in **a** (green filled circles) and from dielectric function fitting to IR reflection spectra (orange filled circles) are also provided and show good agreement with theory, except at the highest enrichment levels.

non-polar E_{2g} phonon lifetime was determined from the Raman linewidth. In all, 16 different hBN crystals were characterized with Raman spectroscopy, five of which are shown in Fig. 1a. A clear spectral shift from the naturally occurring hBN E_{2g} phonon energy (~1,366 cm^{-1}) is found with isotopic enrichment; specifically an increase of 27 cm^{-1} to ~1,393 cm^{-1} for 98.7% h^{10}BN (blue curve, Fig. 1a) and a decrease of 9 cm^{-1} to 1,357 cm^{-1} for 99.2% h^{11}BN (red curve). Although the E_{1u} (TO) phonon is not Raman active, a corresponding spectral shift in the upper Reststrahlen band of similar magnitude is also identified, with the band for each material characterized by the broad, highly reflective regions shown in Fig. 1b. This suggests that both IR- (E_{1u}) and Raman-active (E_{2g}) phonons can be similarly tuned with isotopic concentration, as shown in other semiconductors[18,19,29,30]. In addition, the E_{2g} linewidth narrows significantly with increased isotopic purity, with a minimum linewidth achieved for the hBN samples with the highest enrichments. This minimum linewidth was consistent with an approximately factor of three reduction with respect to the naturally abundant materials (a full table of Raman and SIMS results for all crystals studied are provided in the Supplementary Information). Such a reduction in linewidth is indicative of a commensurate increase in the corresponding phonon lifetime.

The overall increase in E_{2g} phonon lifetime with isotopic purity can be easily discerned from Fig. 1c. In general, phonon lifetimes are limited by intrinsic three-phonon scattering and by disorder scattering from different isotopes. Here we obtained the phonon dispersion relations and the anharmonic interactions between phonons from first-principles density functional theory (DFT), with phonon–isotope scattering represented as mass defects. This approach gives quantitative phonon dispersion relations (for example, Supplementary Fig. 3) and thermal transport constants[31,32]. The results for the Raman-active phonon lifetimes, $\tau_{E_{2g}}$ in bulk hBN obtained in this way are provided in Fig. 1c (open green squares) as a function of ^{11}B concentration, and the experimental lifetimes extracted from the Raman spectra in Fig. 1a are provided for comparison (solid green circles). Good quantitative agreement between theory and experiment is obtained, with the exception of the highest enriched samples (^{11}B concentrations within a few percent of 0% and 100%). For these crystals, the experimentally determined lifetimes appear to saturate near 2 ps, falling short of the ~8 ps values predicted for isotopically pure materials. To understand the reason for this suppression of the phonon lifetime, additional SIMS analysis was performed to determine the carbon and oxygen impurity levels in the isotopically enriched samples with respect to the naturally abundant crystals. Although quantitative values for the oxygen content could not be ascertained, at least two to three orders of magnitude higher carbon concentration was found in the highest enriched samples (see Supplementary Information). Such an increased carbon concentration, especially in the presence of suppressed isotopic scattering, may provide an alternative optical phonon scattering pathway, preventing the predicted 8 ps lifetimes from being realized. Thus, theory implies that even longer phonon lifetimes, and further reductions in optical losses, should be possible if impurity levels can be suppressed.

Just as the isotopically enriched crystals exhibit shifted phonon frequencies, shifted Reststrahlen bands and increased phonon lifetimes (Fig. 1), they also possess infrared dielectric functions unique from the naturally abundant material. In an effort to determine these dielectric functions, reflectance spectra were collected from the original hBN crystals in a Bruker Hyperion 2000 FTIR microscope and fitted using the commercial WVase software from J. A. Woolam. The real and imaginary components of the permittivities extracted from these fits are provided in Figs 2a and 2b, respectively, for the highest enriched (^{11}B 99.2% and ^{10}B 98.7%) and naturally abundant hBN samples.

With an increase in the (Raman-active) E_{2g} phonon lifetime, increases in the (IR-active) E_{1u} phonon lifetime are also anticipated. Such increases in $\tau_{E_{1u}}$ are readily apparent from Fig. 1c (open orange squares). From these calculations, clearly the overall trend in lifetime change with isotopic enrichment and the approximate magnitude of the phonon lifetimes are roughly equivalent for the E_{2g} and E_{1u} phonons. In an effort to provide some experimental evidence for this, $\tau_{E_{1u}}$ was extracted from the TO phonon damping constants derived from the dielectric function fits for the highest enriched and naturally abundant samples, and provided again in Fig. 1c (filled orange circles). Although only three points, again, strong agreement between the theory and experiment and between the Raman- and IR-active phonon lifetimes and trends are observed. Thus, the preponderance of evidence supports both the predicted trends and the upper limits of the phonon lifetimes, and that the Raman linewidths can serve as a reasonable first approximation for the IR-active phonon lifetime.

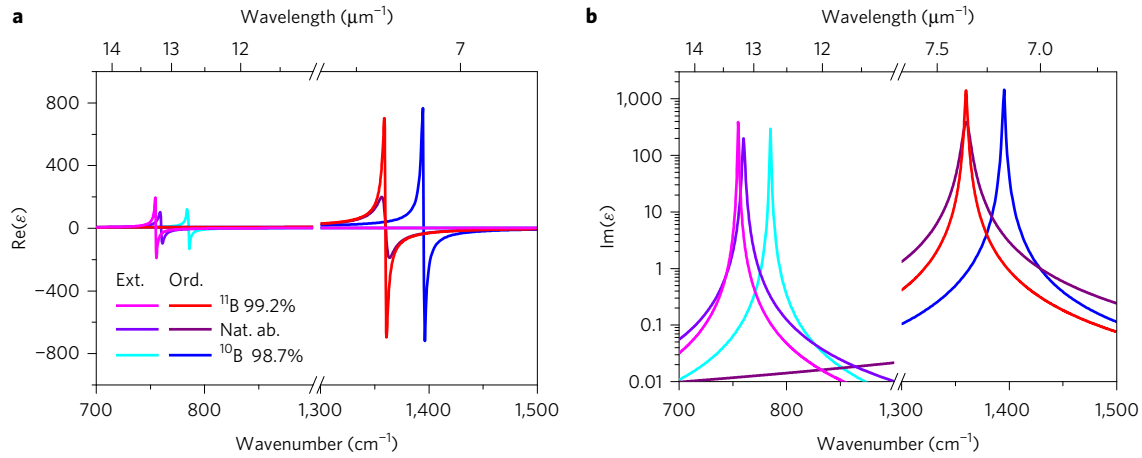

Figure 2 | Influence of isotopic enrichment on hBN dielectric function. a,**b**, Real and imaginary part, respectively, of the dielectric function for hBN for two highly enriched and for naturally abundant material. The values were extracted from reflectance measurements from hBN crystals that were used to exfoliate the flakes investigated by s-SNOM. Ext.—extraordinary; Ord.—ordinary.

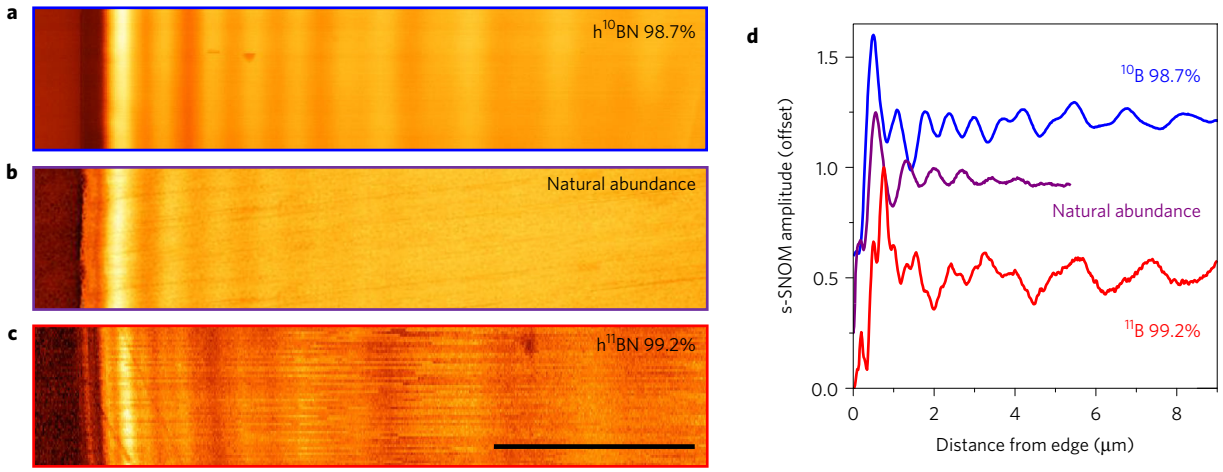

Figure 3 | Measuring polariton propagation as a function of isotopic enrichment. a–**c**, Spatial plots of the scattering-type scanning near-field optical microscope (s-SNOM) measurements collected from ∼120-nm-thick hBN flakes of ^{10}B 98.7% (**a**), naturally abundant (**b**) and ^{11}B 99.2% (**c**). The scale bar represents 5 μm. The polaritons were stimulated with a 1,510, 1,480 and 1,480 cm^{-1} incident laser source, respectively, corresponding to Re(ε) ∼ −6.25 for each. **d**, Linescans extracted from **a** to **c** demonstrate the significantly longer propagation lengths in the enriched in comparison to the naturally abundant flake. The linescans were all normalized and offset so they could be compared on the same scale. Further, the presence of multiple frequency components resulting from higher-order modes can be observed in both the raw spatial plots (**a**–**c**) and the linescans of the enriched samples that are absent from the naturally abundant measurements.

As the optical losses of PhPs in the UR of hBN are intimately tied to the E_{1u} phonon scattering rates, an increase in the phonon lifetime within the enriched samples should also result in similar increases in the propagation lengths of the hyperbolic phonon polaritons (HPhPs) they support. Such increases can be clearly identified in the spatial plots of the PhP propagation within ∼120-nm-thick flakes of the highest isotopically enriched hBN with respect to the similar thickness naturally abundant material (Fig. 3a–c). These spatial plots were acquired using scattering-type, scanning near-field optical microscopy (s-SNOM) techniques described in the Methods and elsewhere[4,5,24]. HPhP propagation is visualized in these experiments by the interference between the SNOM-tip-launched, hBN-flake-edge-launched and hBN-flake-edge-reflected HPhPs, resulting in the oscillatory patterns seen in the spatial plots. By measuring the periodicity of these oscillations, the HPhP wavelength λ_{HPhP}, and therefore the compression of the optical fields (in-plane wavevector q), can be determined. To accommodate for the spectral shifts in the dielectric functions between each of the hBN materials, the s-SNOM plots presented were collected at frequencies where the magnitude of the real part of the dielectric function was approximately the same [Re(ε) ∼ −6.25]. From the qualitative comparisons provided in the corresponding linescans (Fig. 3d) two clear conclusions can be drawn: there is a striking increase in the propagation lengths in the highly enriched samples and additional higher-frequency oscillations are clearly present in the interference patterns observed in the s-SNOM plots collected from these enriched samples as well.

The in-plane wavevector, which also determines the out-of-plane confinement, is given by $q = 2\pi/\lambda_{HPhP}$. From the fast Fourier transform (FFT) of each linescan, λ_{HPhP} can be determined as a function of incident frequency, and thus the magnitude of q can be extracted (see Supplementary Information). The dispersion relationship for the HPhPs can then be determined by plotting q as a function of incident frequency. Comparison of these experimental values with the calculated plots of the HPhP dispersion (Fig. 4) makes clear that the extracted dielectric functions provide a good estimation of the polaritonic behaviour of all three samples, and that these higher-frequency oscillatory components correspond to

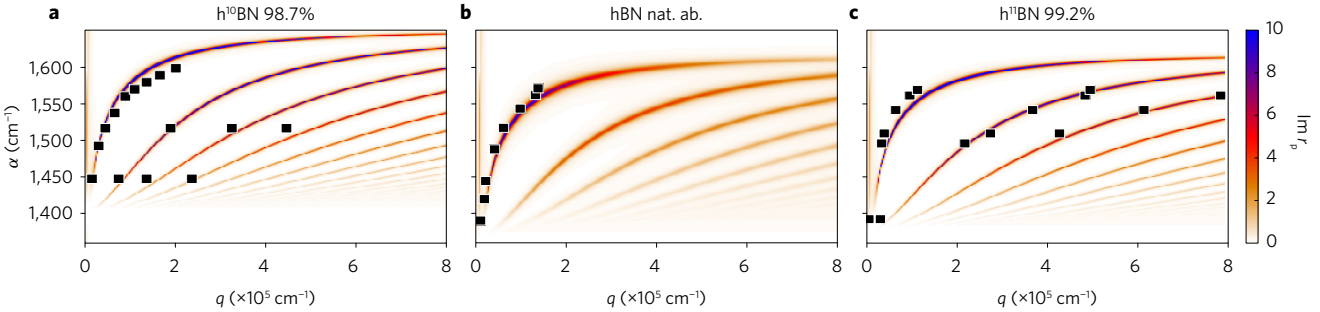

Figure 4 | Dispersion of hyperbolic phonon polaritons in isotopically enriched hBN. a–c, The in-plane wavevector, q, is plotted for the 98.7% ^{10}B (**a**), naturally abundant (**b**) and 99.2% ^{11}B (**c**) hBN flakes in Fig. 3 as a function of incident frequency. The experimentally extracted fundamental and higher-order modes (purple triangles) are superimposed on the calculated dispersion for each using the dielectric functions presented in Fig. 2. The loss is qualitatively represented by the breadth and magnitude of the imaginary part of the reflectivity, r_p, provided in the false-colour plot of the dispersion relation for each crystal type.

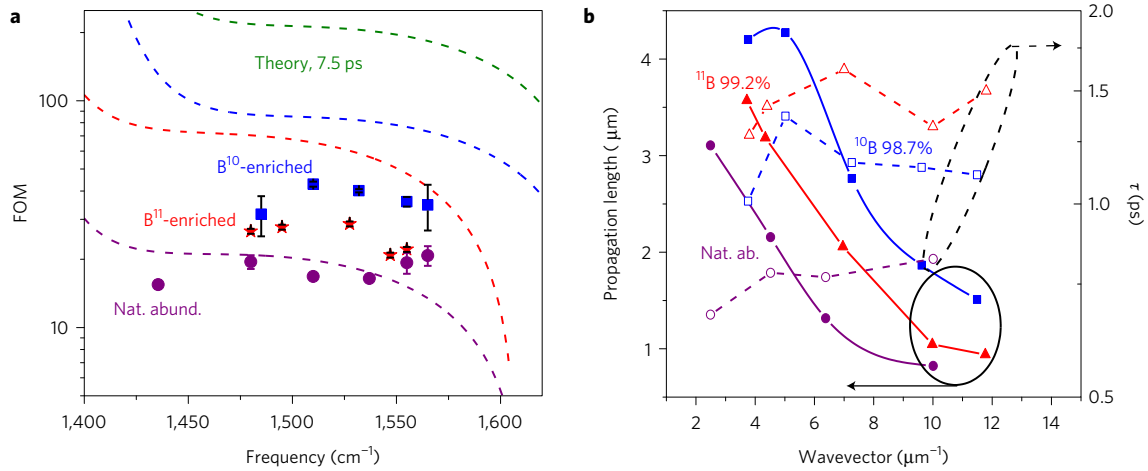

Figure 5 | Quantifying improvements in loss with isotopic enrichments. a, The figure of merit (FOM) as defined in the text is plotted for each of the hBN crystals presented in Fig. 3 as a function of incident frequency. The experimental values, extracted from the linewidth and wavevector of each HPhP mode, are plotted for the ^{10}B 98.7% (blue squares) and ^{11}B 99.2% (red triangles) enriched hBN flakes in comparison to the naturally abundant sample (purple circles). A clear increase in the FOM is observed for the isotopically enriched samples at every frequency measured, showing uniform reduction in loss across the frequency range. Although the values extracted from the naturally abundant flake agree fairly well with the theoretically predicted values calculated from the dielectric function in Fig. 2 (purple dashed line), the values for the isotopically enriched materials fall short of the corresponding theoretical predictions (red and blue dashed lines). For comparison, the FOM was also calculated for a ^{10}B with 100% enrichment using the lifetime calculated for such a case in the absence of additional point defects (green line). **b**, The increases in FOM also result in commensurate increases in the HPhP propagation lengths (left axis), while extracted HPhP lifetimes (right axis) for the three samples agree fairly well with the phonon lifetimes extracted from the Raman linewidth (Fig. 1a).

higher-order HPhPs. In these plots, the false colour corresponds to the theoretically predicted optical losses, while the symbols designate the experimentally determined values from the s-SNOM measurements. Although higher-order modes have been previously reported in three-dimensionally confined hBN nanostructures[12,25] and within naturally abundant flakes of hBN with high-resolution s-SNOM scans[20], in the latter case, those modes were identified only in flakes very close to the pristine, sharp edges, and decayed within a single oscillatory cycle, therefore making quantification of the damping impossible. Here, these higher-order modes can be directly discerned in the s-SNOM plots, with up to three higher-order modes experimentally identified (Fig. 4), each of which was observed to propagate for multiple oscillations. This allowed the associated damping to be quantified and was determined to be similar to the fundamental HPhP modes. The shorter propagation lengths measured are the result of only the shorter λ_{HPhP} associated with the higher-order modes.

Although the s-SNOM plots and linescans provide strong qualitative evidence for increased propagation lengths and reduced HPhP damping, to quantify the improvements, a direct comparison must be realized. A relevant figure of merit (FOM) may be defined simply as $Q = \mathrm{Re}(q)/\mathrm{Im}(q)$, where $\mathrm{Im}(q)$ is proportional to the fitted half-width at half-maximum (HWHM) of the spectral linewidths extracted from the FFT of the s-SNOM linescans. Since the enriched samples displayed both tip- and edge-launched modes with centre frequencies differing by approximately a factor of two, we have applied a numerical filter around the frequency of the tip-launched polariton. The tip-launched, rather than edge-launched peak was chosen because it displayed greater consistency from one data set to another and was generally stronger in amplitude. The filtered frequency-space signal was transformed back to real space, corrected for the geometric-decay factor proportional to $x^{-1/2}$, and transformed again into the frequency space. The HWHM was extracted from a Lorentzian fit to the resulting profile, as illustrated for a few cases in the Supplementary Information. To verify the accuracy of the fitted linewidths from the FFT, direct real-space fits of $\mathrm{Im}(q)$ to the linescans were determined from s-SNOM plots of naturally abundant hBN flakes and were found to be in general quantitative agreement. A full description of this analysis is provided in the Supplementary Information.

Analysis of the propagating FOM for each of the samples at several incident frequencies shows there is a substantial increase in the two isotopically enriched samples (blue squares and red triangles in Fig. 5a) over the naturally abundant response (purple circles). The data indicates that the improvement ranges from ∼50% to almost a factor of three. Although the FOMs are always larger for the enriched samples, the overall magnitude increase is less than predicted using the extracted dielectric functions (dashed red and blue lines in Fig. 5a). There are many potential contributing factors to this apparent suppression of the FOM and propagation length, L_P (left axis, Fig. 5b). Perhaps the most likely reason stems from the significantly smaller size of the enriched flakes (∼10 μm on a side) with respect to the naturally abundant material (>50 μm on a side). This smaller size causes the detected s-SNOM response to consist of two propagating HPhPs, each launched from opposite edges of the flake, that meet and interfere at the flake centre. This causes additional geometrical damping that is not inherent to the material, not present in the larger, natural abundant flakes and is not accounted for in the FOM calculations. Further, this smaller size also made it more difficult to identify flakes of the appropriate thickness that were free from defects and ridges within a propagation length of the edge, resulting in further geometric scattering. Thus, the values presented here for the propagation lengths for the isotopically enriched samples can be considered as a lower limit. Even with these physical limitations, the FOM clearly displays the same trend as the Raman linewidths, the fitted damping constants, and the qualitative analysis of the s-SNOM plots.

Although the comparison of L_P clearly shows an improvement with isotopic enrichment, we can verify that is the case through a more direct comparison of the measured PhP lifetimes to those of the TO phonons. The PhP lifetime, $\tau_{PhP} = L_P/v_g$, where v_g represents the group velocity and is determined by taking the first derivative of the ω–q dispersion relationships (Fig. 4). Since reliable values for L_P were extracted only for the principal mode, we confine the comparison to the first branch of the dispersion relationship. The corresponding τ_{PhP} plot is given in Fig. 5b (right axis). An intriguing result is that although L_P is longer for the $h^{10}BN$ sample, this is compensated by the faster v_g (see Supplementary Information) resulting from the slightly broader Reststrahlen band. This leads to the longer τ_{PhP} in the $h^{11}BN$ material. These τ_{PhP} values are in good agreement with the IR $\tau_{E_{1u}}$ and Raman $\tau_{E_{2g}}$ (Fig. 1c), suggesting τ_{PhP} can indeed approach the upper limit imposed by the phonon lifetimes and be approximated by these measurements.

Through the isotopic enrichment of hBN, we have experimentally demonstrated threefold increases in bulk phonon lifetimes and demonstrate that these correspond to a commensurate and approximately equal increase in both lifetime and propagation length of PhPs over the already low-loss naturally abundant hBN crystals. This occurs despite the presence of other point defects (for example, carbon impurities). Although these enhancements are significant, first-principles calculations predict that over an order of magnitude increase in phonon lifetime is possible, offering similar improvements in the propagating FOM (dashed green line in Fig. 5a). In addition to longer propagation lengths, pronounced higher-order modes were identified and maintained for many oscillations, which may extend the range of polaritonic applications, for instance in higher transmission, spatial resolution and/or resolving power in hBN-based hyperlensing approaches[6,20] or where fine spatial filtering of broad-band spectral components with high transmission efficiency (see Supplementary Information) is desired. Although we have demonstrated the potential of isotopic enrichment for enhancing phonon lifetimes using hBN, this methodology can be equally applied to a broad range of polar dielectric materials, and is widely applicable over a large spectral range. Further, by coupling this approach with other methodologies that offer longer propagation lengths, such as electromagnetic hybrids[6,7,10,33,34], we envisage that high-efficiency, multifunctional polaritonic devices can result, offering novel opportunities for the next generation of infrared optical components.

Methods

Methods, including statements of data availability and any associated accession codes and references, are available in the online version of this paper.

Received 7 March 2017; accepted 1 November 2017; published online 11 December 2017

References

1. Yu, N. & Capasso, F. Flat optics with designer metasurfaces. *Nat. Mater.* **13,** 139–150 (2014).
2. Kildishev, A. V., Boltasseva, A. & Shalaev, V. M. Planar photonics with metasurfaces. *Science* **339,** 1232009 (2013).
3. Li, P. *et al*. Reversible optical switching of highly confined phonon polaritons with an ultrathin phase-change material. *Nat. Mater.* **15,** 870–875 (2016).
4. Chen, J. *et al*. Optical nano-imaging of gate-tunable graphene plasmons. *Nature* **487,** 77–81 (2012).
5. Fei, Z. *et al*. Gate-tuning of graphene plasmons revealed by infrared nano-imaging. *Nature* **487,** 82–85 (2012).
6. Dai, S. *et al*. Graphene on hexagonal boron nitride as an tunable hyperbolic metamaterial. *Nat. Nanotech.* **10,** 682–686 (2015).
7. Caldwell, J. D. *et al*. Atomic-scale photonic hybrids for mid-infrared and terahertz nanophotonics. *Nat. Nanotech.* **11,** 9–15 (2016).
8. Spann, B. T. *et al*. Photoinduced tunability of the reststrahlen band in 4H-SiC. *Phys. Rev. B* **93,** 085205 (2016).
9. Khurgin, J. B. How to deal with the loss in plasmonics and metamaterials. *Nat. Nanotech.* **10,** 2–6 (2014).
10. Caldwell, J. D. *et al*. Low-loss, infrared and terahertz nanophotonics with surface phonon polaritons. *Nanophotonics* **4,** 44–68 (2015).
11. Caldwell, J. D. *et al*. Low-loss, extreme sub-diffraction photon confinement via silicon carbide surface phonon polariton nanopillar resonators. *Nano Lett.* **13,** 3690–3697 (2013).
12. Caldwell, J. D. *et al*. Sub-diffractional, volume-confined polaritons in the natural hyperbolic material hexagonal boron nitride. *Nat. Commun.* **5,** 5221 (2014).
13. Wang, T., Li, P., Hauer, B., Chigrin, D. N. & Taubner, T. Optical properties of single infrared resonant circular microcavities for surface phonon polaritons. *Nano Lett.* **13,** 5051–5055 (2013).
14. Low, T. *et al*. Polaritons in layered two-dimensional materials. *Nat. Mater.* **16,** 182–194 (2017).
15. Basov, D. N., Fogler, M. M. & Garcia de Abajo, F. J. Polaritons in van der Waals materials. *Science* **354,** 195–203 (2016).
16. Wang, T. *et al*. Phononic bowtie nanoantennas: controlling ultra-narrow-band infrared thermal radiation at the nanoscale. *ACS Photon.* **4,** 1753–1760 (2015).
17. Yoxall, E. *et al*. Direct observation of ultraslow hyperbolic polariton propagation with negative phase velocity. *Nat. Photon.* **9,** 674–678 (2015).
18. Cardona, M. & Thewalt, M. L. W. Isotope effects on the optical spectra of semiconductors. *Rev. Mod. Phys.* **77,** 1173–1224 (2005).
19. Khurgin, J. B., Jena, D. & Ding, Y. J. Isotope disorder of phonons in GaN and its beneficial effect on high power field effect transistors. *Appl. Phys. Lett.* **93,** 032110 (2008).
20. Dai, S. *et al*. Subdiffractional focusing and guiding of polaritonic rays in a natural hyperbolic material. *Nat. Commun.* **6,** 6963 (2015).
21. Liu, Z., Lee, H., Xiong, Y., Sun, C. & Zhang, X. Far-field optical hyperlens magnifying sub-diffraction limited objects. *Science* **315,** 1686 (2007).
22. Xiong, Y., Liu, Z. & Zhang, X. A simple design of flat hyperlens for lithography and imaging with half-pitch resolution down to 20 nm. *Appl. Phys. Lett.* **94,** 203108 (2009).
23. Kumar, A., Low, T., Fung, K. H., Avouris, P. & Fang, N. X. Tunable light-matter interaction and the role of hyperbolicity in graphene-hBN system. *Nano Lett.* **15,** 3172–3180 (2015).
24. Dai, S. *et al*. Tunable phonon polaritons in atomically thin van der Waals crystals of boron nitride. *Science* **343,** 1125–1129 (2014).
25. Giles, A. J. *et al*. Imaging of anomalous internal reflections of hyperbolic phonon-polaritons in hexagonal boron nitride. *Nano Lett.* **16,** 3858–3865 (2016).
26. Poddubny, A., Iorsh, I., Belov, P. & Kivshar, Y. Hyperbolic metamaterials. *Nat. Photon.* **7,** 948–957 (2013).

27. Kubota, Y., Watanabe, K., Tsuda, O. & Taniguchi, T. Deep ultraviolet light-emitting hexagonal boron nitride synthesized at atmospheric pressure. *Science* **317,** 932–934 (2007).
28. Hoffmann, T. B., Zhang, Y., Edgar, J. H. & Gaskill, D. K. Growth of hBN using metallic boron: isotopically enriched h10BN and h11BN. *MRS Proc.* **1635,** 35–40 (2014).
29. Zhang, J. M. *et al*. Raman spectra of isotopic GaN. *Phys. Rev. B* **56,** 14399–14406 (1997).
30. Rohmfeld, S., Hundhausen, M., Ley, L., Schulze, N. & Pensl, G. Isotope-disorder-induced line broadening of phonons in the Raman spectra of SiC. *Phys. Rev. Lett.* **86,** 826–829 (2001).
31. Lindsay, L., Broido, D. A. & Reinecke, T. L. Ab-initio thermal transport in compound semiconductors. *Phys. Rev. B* **87,** 165201 (2013).
32. Lindsay, L., Broido, D. A. & Reinecke, T. L. Phonon-isotope scattering and thermal conductivity in materials with a large isotope effect: a first-principles study. *Phys. Rev. B* **88,** 144306 (2013).
33. Caldwell, J. D. & Novoselov, K. S. van der Waals heterostructures: mid-infrared nanophotonics. *Nat. Mater.* **14,** 364–366 (2015).
34. Woessner, A. *et al*. Highly confined low-loss plasmons in graphene–boron nitride heterostructures. *Nat. Mater.* **14,** 421–425 (2015).

Acknowledgements

A.J.G. and C.T.E. acknowledge support from the National Research Council (NRC) and I.C. acknowledges support from the American Society of Engineering (ASEE) NRL Postdoctoral Fellowship Programs. Funding for N.A. was provided through the Naval Research Enterprise Internship Program (NREIP) and is currently an undergraduate student at Rice University in Houston, Texas. Funding for J.D.C., I.V., J.G.T. and T.L.R. was provided by the Office of Naval Research and distributed by the Nanoscience Institute at the Naval Research Laboratory. Development of the instrumentation is supported by ARO w911NF-13-1-0210 and AFOSR FA9550-15-0478. D.N.B. is the Moore Investigator in Quantum Materials EPIQS program GBMF4533. D.N.B., M.M.F. and S.D. acknowledge support from ONR N00014-15-1-2671. The hBN crystal growth at Kansas State University was supported by NSF grant CMMI 1538127. L.L. acknowledges support from the US Department of Energy, Office of Science, Office of Basic Energy Sciences, Materials Sciences and Engineering Division. SIMS measurements and analysis was provided by Evans Analytical Group as part of a work-for-hire agreement. The authors express their thanks to K. Wahl for use of her Raman microscope. The United States Government retains and the publisher, by accepting the article for publication, acknowledges that the United States Government retains a non-exclusive, paid-up, irrevocable, world-wide licence to publish or reproduce the published form of this manuscript, or allow others to do so, for United States Government purposes. The Department of Energy will provide public access to these results of federally sponsored research in accordance with the DOE Public Access Plan (http://energy.gov/downloads/doe-public-access-plan).

Author contributions

The concept for the experiment was initially developed by J.D.C., A.J.G., T.L.R. and I.V. All hBN crystals were grown by T.H. and S.L. under the direction of J.E. and provided to J.D.C. through an amazing stroke of good fortune. Exfoliation of hBN flakes was performed by J.D.C. and A.J.G., while AFM characterization was provided by A.J.G. Raman and FTIR analysis was provided by J.D.C., A.J.G., N.A., I.C., C.T.E. and J.G.T. Theoretical calculations of the phonon lifetimes were performed by L.L. and T.L.R., while the code for calculating the dispersion relationship of the HPhPs in hBN was developed by M.F. The FFTs and corresponding lineshape fits were created by I.V. s-SNOM measurements were performed within the lab of D.N.B. by A.J.G. and S.D. All authors discussed results at all stages and participated in the development of the manuscript. A.J.G. and J.D.C. wrote the paper.

Additional information

Supplementary information is available in the online version of the paper. Reprints and permissions information is available online at www.nature.com/reprints. Publisher's note: Springer Nature remains neutral with regard to jurisdictional claims in published maps and institutional affiliations. Correspondence and requests for materials should be addressed to A.J.G.

Competing financial interests

The authors declare no competing financial interests.

Methods

hBN Growth. Hexagonal boron nitride crystals were precipitated from a nickel-chromium flux at atmospheric pressure.

Crystal growth of hBN with the natural distribution of isotopes. hBN crystals with the natural distribution of isotopes (20% B-10 and 80% B-11) were produced using a hot-pressed boron nitride ceramic boat, which served as both the container for the metal flux and as the B and N sources. The flux was a mixture of 50 wt% Ni and 50 wt% Cr powders. After loading the crucible, the furnace was evacuated, then filled with N_2 and forming gas (5% hydrogen in balance argon) to ∼850 torr. The N_2 and forming gases continuously flowed through the system during crystal growth with flow rates of 125 sccm and 25 sccm, respectively. The system was heated to 1,550 °C for a dwell time of 24 h. The hBN crystals were formed by cooling at a rate of 1 °C h^{-1} to 1,500 °C, then quenching the process to room temperature. In our experiments, forming gas was used to minimize oxygen and carbon impurities that are recognized as the main contaminants in hBN crystals.

B^{10} and B^{11}-enriched hBN crystal growth method. Since hot-pressed boron nitride ceramics are available only with the natural distribution of boron isotopes, to grow isotopically pure hBN crystals, the procedure had to be modified to use elemental boron as a source material. Therefore, the boron nitride boat was replaced with an alumina crucible. High-purity ^{10}B (99.22 at%) or ^{11}B (99.41 at%) powders were mixed with Ni and Cr powders to give overall concentrations of 4 wt% B, 48 wt% Ni and 48 wt% Cr. In this case, all nitrogen in the hBN originated from the flowing N_2 gas. Other than these changes, the procedure was the same as described above.

Raman measurements. Raman measurements were performed using the 532 nm laser line of an argon-ion laser within a Renishaw Raman microscope. The <10 mW laser line was directed at the sample through a 50×, 0.75 NA objective, with the Raman scattered light being collected back through the same objective. The scattered light was dispersed using a 2,400 groove mm^{-1} grating onto a silicon charge-coupled device (CCD). The spectral position of the Raman lines was calibrated against an internal silicon reference sample. For each different hBN sample studied, six measurements were performed with the average spectral position, linewidth and standard deviations reported (Supplementary Information).

FTIR measurements. Infrared reflectance measurements were performed using a Bruker Hyperion microscope coupled to a Bruker Vertex FTIR spectrometer. The measurements were performed using a 15× Cassegrain objective and were collected with a spectral resolution of 2 cm^{-1}. The reflectance spectra reported were all in reference to an aluminium mirror.

Extracting the dielectric function. The dielectric function was extracted for the three crystals with ^{10}B 98.8%, ^{11}B 98.7% and naturally abundant boron isotope concentrations. This was performed using the infrared reflectance spectra collected from the hBN crystals described above. The WVASE software (J.A. Woolam) was used to perform the fitting of the reflection spectra, and therefore extract an accurate estimation of the infrared dielectric function. A biaxial model was used with two 'TO–LO' oscillators chosen, one each for the ordinary and extraordinary components. Starting values were taken from those originally reported in our prior work[12] and from the spectral positions of the TO phonons and corresponding linewidths extracted from the Raman measurements of the same crystals. The best fit parameters are provided in the Supplementary Information.

Phonon lifetime calculations. Bulk hBN lattice parameters ($a = 2.478$ Å; $c = 6.425$ Å) were determined for the AA' stacking configuration from electronic structure energy minimization using density functional theory in the local density approximation. The harmonic forces, Born charges and dielectric tensor that govern phonon dispersions, including LO/TO splitting from long-range Coulomb forces, were determined from density functional perturbation theory, while the anharmonic forces that govern intrinsic phonon interactions were calculated from perturbations of the electronic structure in large supercells. Transition probabilities for anharmonic three-phonon interactions and phonon–isotope interactions are determined from Fermi's golden rule and summed; inverting this gives the phonon lifetimes.

s-SNOM measurements and analysis. The s-SNOM measurements were performed by focusing the tunable infrared radiation from a Daylight Solutions MirCAT quantum cascade laser system onto the metallized atomic force microscope (AFM) tip of the NeaSpec s-SNOM instrument. Incident light scatters off of the tip, as well as the edge of the hBN flake, providing the necessary change in momentum[12,24] to launch propagating HPhPs provided the light source is within the Reststrahlen band of the hBN. Due to lack of monochromatic laser sources in the LR, our measurements are limited to the UR. The peak-to-peak distance of the interference fringes observed within the s-SNOM spatial plots is equal to λ_{HPhP} and $\lambda_{HPhP}/2$ for the edge- and tip-launched modes, respectively. Plotted in Fig. 3a–c are the s-SNOM plots collected at 1,510, 1,480 and 1,480 cm^{-1} for the ∼120-nm-thick ^{10}B enriched, naturally abundant, and ^{11}B enriched flakes, for which $\mathrm{Re}(\varepsilon) = -6.20$, -6.25 and -6.3, respectively. The strong dispersion in this regime requires that we image at (or close to) identical permittivity values, which due to the spectral shift in the optical phonons with changing isotopic mass occur at different frequencies for each of the different samples studied. Furthermore, since the dispersion of the HPhP modes of hBN is strongly thickness dependent, the presented s-SNOM results were all collected from 118- to 120-nm-thick flakes on a 280-nm-thick SiO_2-on-Si substrate.

Data availability. The data that support the findings of this study are available from the corresponding author upon reasonable request.

nature materials

SUPPLEMENTARY INFORMATION

DOI: 10.1038/NMAT5047

In the format provided by the authors and unedited.

Ultra Low Loss Polaritons in Isotopically Pure Boron Nitride

Alexander J. Giles,[1] Siyuan Dai,[2] Igor Vurgaftman,[1] Timothy Hoffman,[3] Song Liu,[3] Lucas Lindsay,[4] Chase T. Ellis,[1] Nathanael Assefa,[5] Ioannis Chatzakis,[6] Thomas L. Reinecke,[1] Joseph G. Tischler,[1] Michael M. Fogler,[2] J.H. Edgar,[3] D.N. Basov,[2,7] Joshua D. Caldwell[8]

I. Secondary Ion Mass Spectroscopy

To quantify the exact isotope ratios in different samples, we employed secondary ion mass spectroscopy (SIMS) performed by Evans Analytical Group. The relationship between the boron isotope fraction and the Raman peak position is plotted in **Fig. S1**. As a means to simply quantify the relationship between the two, a linear fit is provided. A more accurate description of the relationship can be provided through approaches such as the coherent potential approximation,[1] however, as all enrichment levels for each sample provided were determined via SIMS, this additional analysis is outside of the scope of this work. SIMS analysis also allowed us to determine the concentration of elemental carbon in the hBN samples (**Table S1**), which was shown to be several orders of magnitude higher in isotopically pure crystals. While the exact increase could not be determined directly due to the concentration in the naturally abundant samples being below the detection limit (on the order of 10^{18} cm^{-3}), for the highest enriched samples these concentrations were at a minimum on the order of 2 orders of magnitude higher. This carbon contamination is perhaps the cause of suppressed lifetimes in high-purity samples, and reducing it is a promising avenue to achieve further increases in phonon and phonon polariton (PhP) lifetimes in future research.

[1]United States Naval Research Laboratory, Washington, DC. [2]Dept. of Physics, University of California San Diego, San Diego, CA. [3]Dept. of Chemical Engineering, Kansas State University, Manhattan, KS. [4]Materials Science and Technology Division, Oak Ridge National Laboratory, Oak Ridge, TN. [5]NREIP Summer Student residing at NRL, Washington, DC. [6]ASEE Postdoctoral Fellow residing at NRL, Washington, DC. [7]Department of Physics, Columbia University, New York, NY. [8]Vanderbilt University, Nashville, TN.

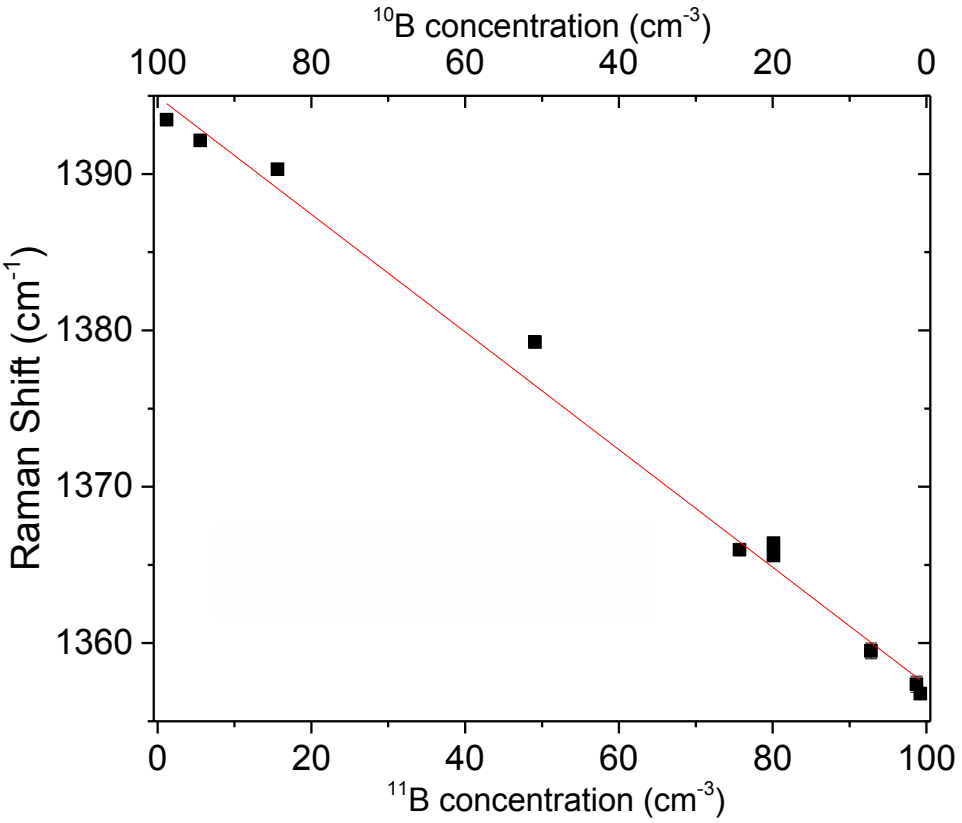

Figure S1: Boron isotope ratio vs. Raman peak position.

h^{10}BN	h^{11}BN	Carbon (cm^{-3})	First 120 nm C (cm^{-3})
0.8	99.2	7.5E+19	1.66E+20
19.9	80.1	<DL	2.58E+19
50.9	49.1	<DL	3.06E+19
98.7	1.3	2.7E+20	9.04E+20

Table S1: Carbon impurity concentration as determined by SIMS. The concentrations are reported as both the average value within the entire sampled depth (~750 nm) and within the first 120 nm from the surface of the crystal.

II. Raman spectroscopy

Raman spectra were collected for a series of hexagonal boron nitride (hBN) crystals with varying isotopic purity in an effort to quantify the influence on the phonon frequency and linewidth. Spectra for five such crystals are plotted in **Fig. 1a** of the main text. The linewidth of the phonon peaks were calculated as the full width at half maximum (FWHM) and are given in **Table S2**.

$h^{10}BN$ %	$h^{11}BN$ %	Raman Shift	σ(Raman Shift)	FWHM	σ(FWHM)
0.8%	99.2%	1356.77	0.134	3.25	0.057
1.3%	98.7%	1357.37	0.517	3.63	0.228
7.2%	92.8%	1359.5	0.5	3.85	0.215
19.9%	80.1%	1365.6	0.235	8.34	0.304
19.9%	80.1%	1366.39	0.219	7.77	0.107
50.9%	49.1%	1379.25	0.358	7.6	0.014
84.4%	15.6%	1390.3	0.14	4.52	0.016
94.4%	5.6%	1392.15	0.109	3.32	0.061
98.7%	1.3%	1393.47	0.259	3.33	0.232

Table S2: Raman peak positions (Raman shift), peak widths (FWHM) and standard deviations (σ) for different isotopic ratios of hBN. Isotopic ratios are determined via secondary ion mass spectroscopy (SIMS). The samples used for the SNOM experiments are highlighted.

III. First Principles Calculations of the Phonon Lifetimes

These calculations employed first principles density functional theory methods to accurately determine phonon dispersions and lifetimes limited by anharmonic phonon-phonon and phonon-isotope scattering from quantum perturbation theory, all with no adjustable parameters. This approach has demonstrated good quantitative agreement with measured data for phonon dispersions and thermal conductivities of a range of non-metallic materials.[2-4] Below we provide details relevant to the hBN calculations given here.

We employ density functional theory within the local density approximation as implemented by the Quantum Espresso package[5] to determine structure, phonon

dispersion and anharmonic couplings for bulk hBN. Ground state electronic structure calculations (12 x 12 x 8 *q*-grids; 110 Ryd plane wave cutoff) for the *AA'* stacking configuration give in-plane and out-of-plane lattice parameters a = 2.478 Å and c = 6.425 Å. Harmonic interatomic force constants (IFCs), Born effective charges and the high frequency dielectric tensor were determined from density functional perturbation theory (8 x 8 x 6 *k*-grid). These determine the long range Coulombic interactions and subsequent splitting of the longitudinal and transverse optic branches[6]. **Figure S3** below gives the calculated phonon dispersion, which is in good agreement with available experimental data. Anharmonic IFCs were determined by Γ-point only electronic structure calculations in perturbed 200 atom supercells with interactions to 3rd nearest neighbors and to nearest neighbor layers.

With the phonon dispersion and anharmonic IFCs as inputs, the phonon lifetimes are determined from first order perturbation theory for each isotope concentration. Third-order anharmonicity[3,7] and isotope mass variances[8-10] are perturbations that give phonon transitions using Fermi's golden rule. Again, this scattering formalism has no adjustable parameters and has demonstrated good agreement with phonon lifetimes[11-13] and thermal conductivity measurements[2-4] for a variety of different systems.

IV. Extraction of the Infrared Dielectric Function

The infrared dielectric function of hBN has been reported elsewhere for naturally abundant materials.[14,15] However, the spectral shift and reduced damping of the optic phonons with increasing isotopic enrichment has not previously been quantified. The real and imaginary parts of the permittivity for the two highest enriched and naturally abundant crystals are provided in the **Fig. 2a** and **b** of the main text and were used to perform the theoretical calculations of the predicted dispersion relationships (**Fig. 4**), figures of merit (FOM) (**Fig. 5a**), and propagation lengths (**Fig. 5b**). To determine these quantities, reflection spectra covering a spectral range including both the upper (UR) and lower Reststrahlen (LR) bands of hBN were collected using a Hyperion 2000 Infrared microscope attached to a Vertex 70v Fourier Transform Infrared spectrometer.

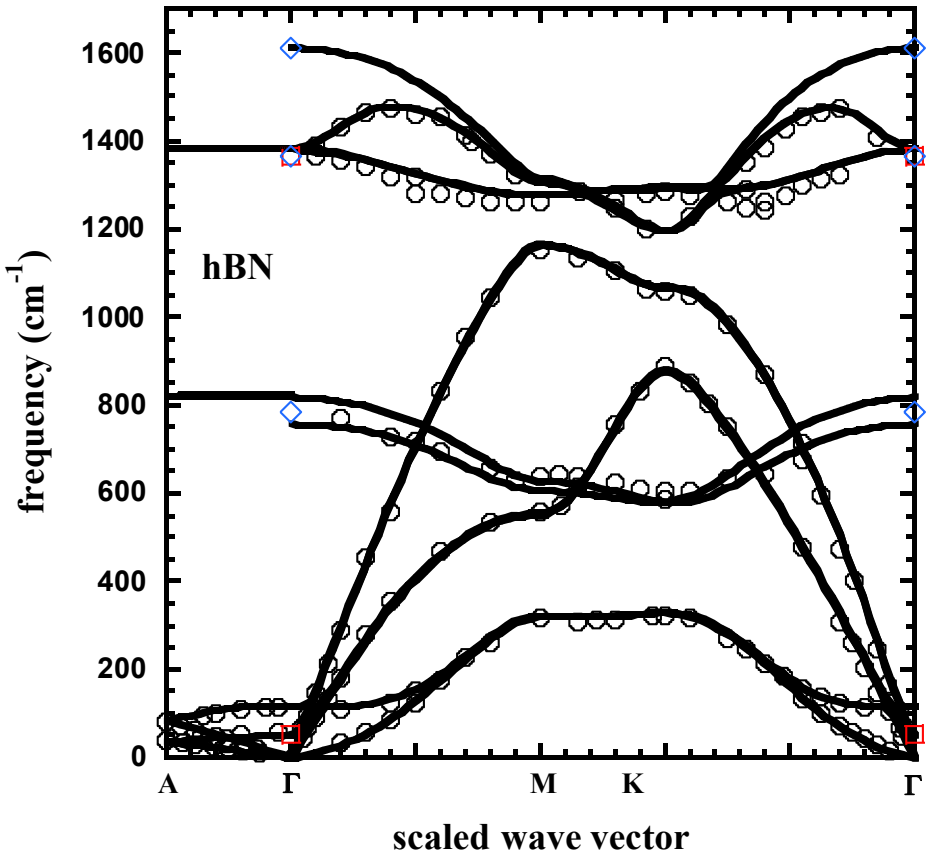

Figure S3: Calculated phonon dispersion of bulk hBN (black curves) compared with measured data from Raman (red squares)[16], IR (blue diamonds)[17] and x-ray (black open circles)[18] experiments.

This was collected using a 15x Cassegrain objective resulting in an incident angle between 11-23°, with a weighted average of ~15°.

Least-squares fitting to the infrared reflection spectra was performed using the commercial WVase software from J.A. Woolam Inc. assuming a general oscillator of the "TOLO" form. The functional form of this is as follows:

$$\varepsilon(\omega) = \varepsilon_{\infty}\left(\frac{\omega_{LO}^2 - \omega^2 - i\Gamma\omega}{\omega_{TO}^2 - \omega^2 - i\Gamma\omega}\right) \quad \text{(S3)}$$

where ω, ω_{TO}, ω_{LO}, $\Gamma$and ε_{∞} represent the frequency, the TO and LO phonon frequencies, the phonon damping and the high-frequency permittivity. An initial

fit was performed for reflectance spectral collected from the crystal source for the naturally abundant hBN flakes discussed in the main text. The extracted fitting parameters were found to be in good agreement with the literature and the above-mentioned Raman spectra. Using the in-plane TO phonon frequencies and linewidths determined from the Raman measurements for the isotopically enriched crystals as an initial starting estimate of the fitting parameters, least-squares fitting was performed. The extracted dielectric functions were found to be in excellent quantitative agreement with the polariton dispersions plotted in **Fig. 4** of the main text, indicating that these provide a good estimation of the material infrared response. A summary of the fitting parameters is provided in **Table S4**.

Ordinary	ε_∞	ω_{TO}(cm^{-1})	ω_{LO}(cm^{-1})	Γ(cm^{-1})
Caldwell et al.[14]	4.98	1362.7	1616.9	7.3
Nat. Ab	4.9	1360	1614	7
^{11}B 99.2%	5.32	1359.8	1608.7	2.1
^{10}B 98.7%	5.1	1394.5	1650	1.8
Ext. Ord.	ε_∞	ω_{TO}(cm^{-1})	ω_{LO}(cm^{-1})	Γ(cm^{-1})
Caldwell et al.[14]	2.95	760	825	3
Nat. Ab	2.95	760	825	3
^{11}B 99.2%	3.15	755	814	1
^{10}B 98.7%	2.5	785	845	1

Table S4: Summary of infrared dielectric function fits for the most recent literature reported values in comparison to the naturally abundant, and the isotopically enriched ^{11}B and ^{10}B hBN crystals discussed in the main text.

V. Figure of Merit Calculations

The measured line-scan data were extracted from the scattering-type scanning near-field microscopy (s-SNOM) plots. An example of such a plot is presented in **Fig. S5a**. This data set was Fourier transformed into the spatial-frequency domain (**Fig. S5b**). Since the tip-launched and edge-launched signals are both

present in the data (double peaks near 1.5 and 1.8 μm^{-1} in **Fig. S5b**), we applied a Lorentzian filter centered around the frequency of the tip-launched polariton mode as determined from a best fit to the raw Fourier transform. The tip-launched (rather than the edge-launched) peak was chosen because it displayed greater consistency from one data set to another and was generally stronger in amplitude. The filtered signal was transformed back to real space and corrected for the geometric-decay factor expected for the circular waves of the tip-launched polariton (i.e. $x^{-1/2}$). The filtered and corrected tip-launched signal was Fourier transformed back to frequency space and fitted with the Lorentzian function to extract the center frequency [Re(q)] and the HWHM [Im(q)] as in **Fig. S5c**. The width of the original frequency filter was adjusted until the damping rate, Im(q), converged to its final value.

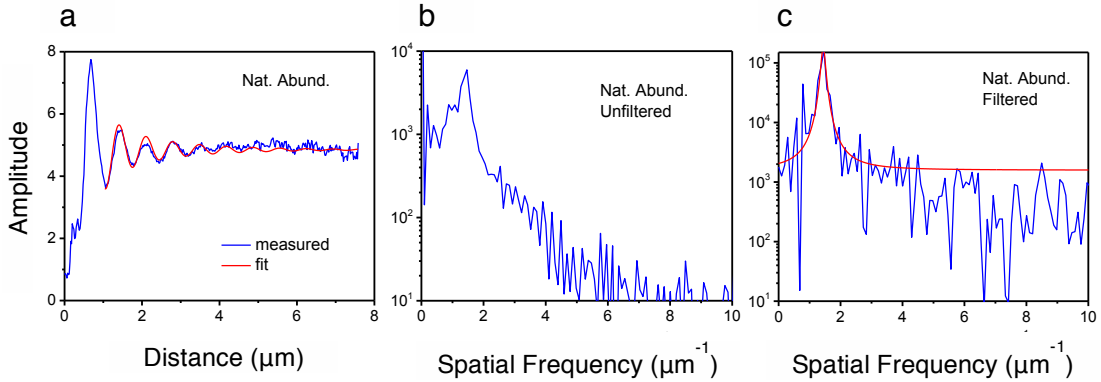

Figure S5: **a** Line-scan data from s-SNOM scans (blue) and fit (red) of a naturally abundant hBN flake. **b** FFT of line-scan data (unfiltered). **c** Filtered FFT of the line scan shown in b (blue), with a Lorentzian fit (red). The figure of merit was calculated from the HWHM of the Lorentzian fit.

VI. Additional Scattering in Isotopically Enriched Flakes

As described in the main text, the smaller size, non-parallel edges and location of additional defects on the isotopically enriched hBN flakes are a potential source of additional scattering. The impact of such scattering on the large-area s-SNOM spatial plots is presented in **Fig. S6 a** and **b** for ^{10}B and ^{11}B enriched flakes discussed in the main text, respectively. Note that in **a**, the interference fringes resulting from tip- and edge-launched polaritons from opposite edges are non-parallel and propagate distances sufficient to interfere with one another near the center of the flake. This induces additional apparent damping resulting in shorter polariton propagation lengths. However, these reductions would not be

anticipated in larger-area flakes where the edges are separated by multiple propagation lengths. In the case of **b**, a similar effect is also observed, albeit due to additional polariton launching and scattering from a ridge on the surface of the flake. Neither of these effects was present in the naturally abundant flakes due to the significantly larger lateral dimensions and shorter propagation lengths associated with this material. It is anticipated that with improved growth of isotopically enriched hBN materials, larger flake sizes and lower impurity concentrations can be realized. In this case, the measured propagation lengths and FOMs are anticipated to approach the values predicted by the extracted infrared dielectric functions, as is the case for the naturally abundant crystals.

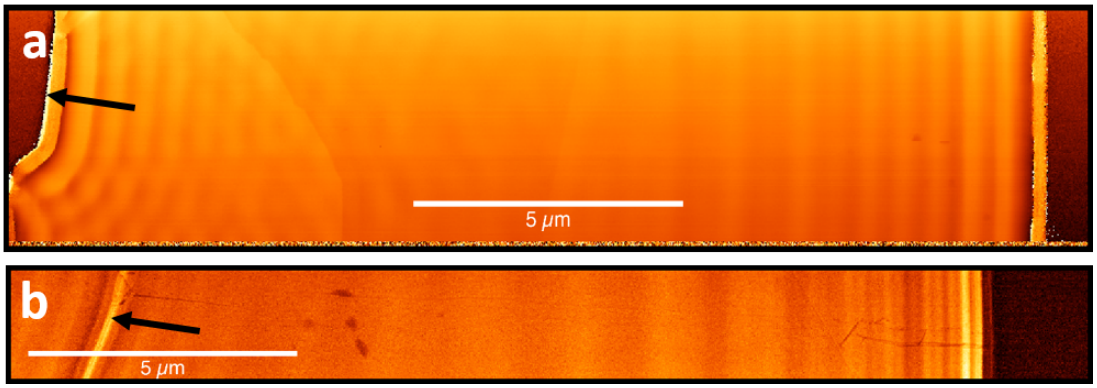

Figure S6: Influence of non-parallel polariton reflections upon propagation. s-SNOM spatial plot collected from the **a** ^{10}B hBN flake at 1510 cm^{-1} and **b** ^{11}B hBN flake at 1480 cm^{-1}. The s-SNOM results presented in **Fig. 3** were taken from the right edge.

VII. Group Velocity and Phonon Polariton Lifetime

In an effort to calculate the polariton lifetimes, the group velocities, V_g as a function of in-plane wavector, q were determined numerically. This was performed by taking the slope of the frequency-dispersion plots in **Fig. 4** $(\delta\omega/\delta q)$ of the main text for the principal mode. This was converted to units of angular frequency. The values for V_g determined at the incident frequencies where reliable propagation lengths were reported (**Fig. 5b**) are presented here as **Fig. S7**. Note that due to variations in the LO-TO phonon splitting, and therefore the widths of the corresponding Reststrahlen bands, differences in V_g exist. These differences are expressed in the different calculated phonon polariton lifetimes in **Fig. 5b**, where despite the longer propagation lengths, L_p (at constant q) for the 98.7% h^{10}BN with respect to the 99.2% h^{11}BN enriched sample, the faster V_g for the former results in a slightly shorter lifetime.

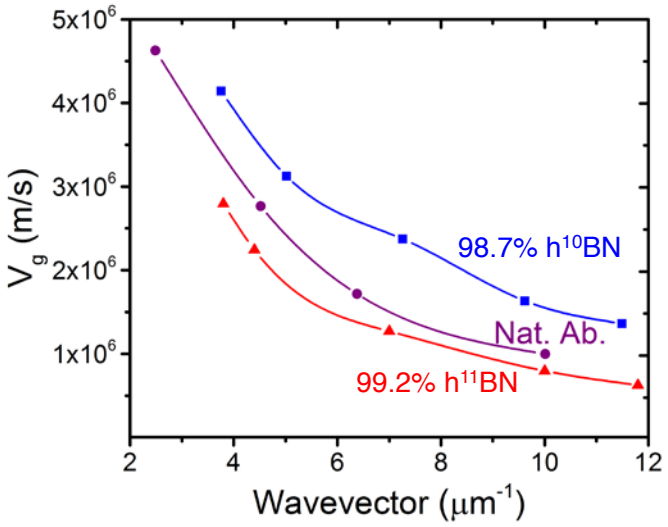

Figure S7: Group velocity for samples studied. Numerically calculated group velocities using dispersion relationships for principal mode in **Fig. 4** along with propagation lengths from **Fig. 5b**.

VIII. Predicted Absorption

We calculated the absorbed fraction of the light upon a single pass through a 100-nm-thick hBN flake using the dielectric functions of the naturally occurring hBN, 98.7% $h^{10}BN$ and 99.2% $h^{11}BN$. We further calculated the absorption of a high-purity $h^{10}BN$ flake with a 7.5 ps lifetime, which roughly corresponds to the theoretically predicted losses for a 100% enriched mateiral. The results are plotted in **Fig S8**. The reduced absorption associated with the longer phonon lifetime achieved via isotopic enrichment demonstrates the strong potential for many nanophotonic optics designs including hyperlensing.

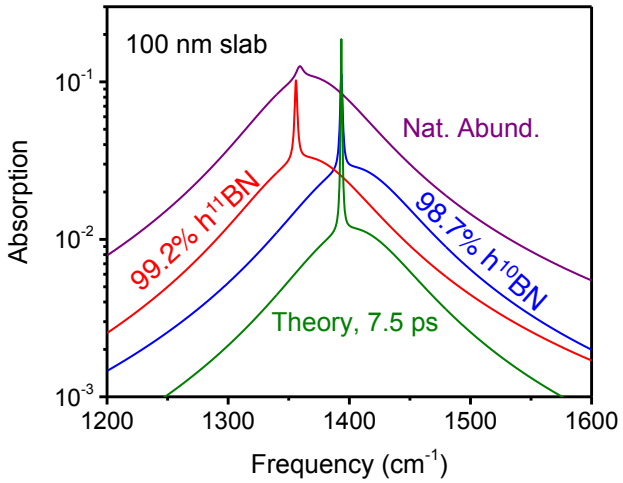

Figure S8: Calculated absorption of naturally abundant hBN (purple), 99.2% $h^{11}BN$ (red), 98.7% $h^{10}BN$ (blue) and 100% $h^{10}BN$ with theoretically predicted optic phonon lifetimes (green).

IX. E_{1u} and E_{2g} Phonon modes near 1366 cm^{-1}

Two phonons exist at 1366 cm^{-1} in naturally abundant hBN, the E_{1u} and E_{2g} modes. The E_{1u} mode has a net dipole change and is thus IR active, while the E_{2g} mode has no net dipole change and is Raman active (**Fig. S9**). While these are distinct phonon modes they are similarly affected by isotope composition; this is demonstrated in **Fig. 1c** which plots DFT calculated lifetimes of both, exhibiting similarly long lifetimes at high isotopic purity (8.34 and 8.47 ps, respectively) and similar trends with changing enrichment. It is important to note that both the E_{1u} and E_{2g} are in-plane shearing modes, occur at similar frequencies and therefore it is not surprising that the resultant magnitude of and trends in lifetime with changing isotopic enrichment are similar. Further, and perhaps most importantly, both exhibit nearly identical spectral shifts at varying isotope fractions, shown in **Fig. 1a** and **b** of the main text.

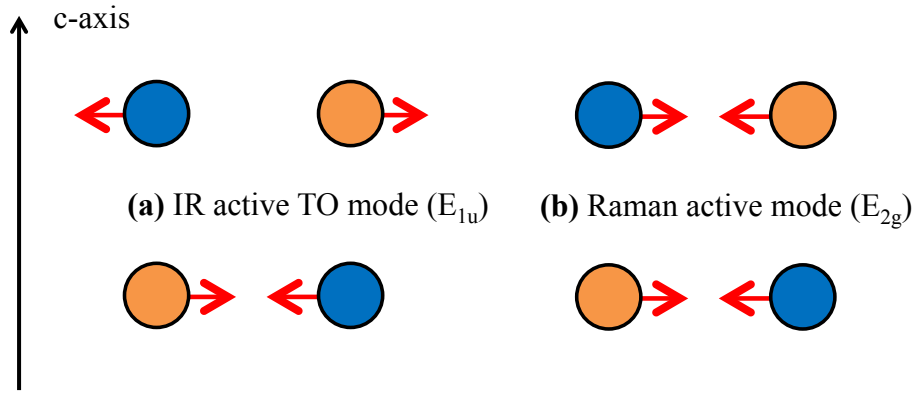

Figure S9: Unit cell displacement patterns for IR active (a) and Raman active (b) high frequency TO phonons.

References

1 Haller, E. E. Isotopically Engineered Semiconductors. *J. Appl. Phys.* **77**, 2857-2878 (1995).

2 Lindsay, L., Broido, D. A. & Reinecke, T. L. Thermal conductivity and large isotope effect in GaN from first principles. *Phys. Rev. Lett.* **109**, 095901 (2012).

3 Lindsay, L., Broido, D. A. & Reinecke, T. L. Ab-initio thermal transport in compound semiconductors. *PhRvB* **87**, 165201 (2013).

4 Lindsay, L. *et al.* Phonon Thermal Transport in Strained and Unstrained Graphene from First Principles. *PhRvB* **89**, 155426 (2014).

5 Quantum Espresso.

6 Baroni, S., de Gironcoli, S., Dal Corso, A. & Giannozi, P. Phonons and related crystal properties from density-functional pertubation theory. *Reviews of Modern Physics* **73**, 515 (2001).

7 Ziman, J. M. *Electrons and Phonons*. (Oxford University Press, 1960).

8 Tamura, S. I. Isotope scattering of dispersive phonons in Ge. *PhRvB* **27**, 858 (1983).

9 Tamura, S. I. Isotope scattering of large-wave-vector phonons in GaAs and InSb - Deformation-dipole and overlap-shell models. *PhRvB* **30**, 849-854 (1984).

10 Lindsay, L., Broido, D. A. & Reinecke, T. L. Phonon-isotope scattering and thermal conductivity in materials with a large isotope effect: A first-principles study. *PhRvB* **88**, 144306 (2013).

11 Debernardi, A., Baroni, S. & Molinari, E. Anharmonic phonon lifetimes in semiconductors from density functional pertubation theory. *Physical Review Letters* **75**, 1819 (1995).

12 Debernardi, A., Ulrich, C., Cardona, M. & Svassen, K. Pressure dependence of Raman linewidth in semiconductors. *Physica Status Solidi B* **223**, 213 (2001).

13 Deinzer, G., Birner, G. & Strauch, D. Ab initio calculation of the linewidths of various phonon modes in germanium silicon. *Physical Review B* **67**, 144304 (2003).
14 Caldwell, J. D. *et al.* Sub-diffractional, Volume-confined Polaritons in the Natural Hyperbolic Material Hexagonal Boron Nitride. *Nature Communications* **in press** (2014).
15 Geick, R., Perry, C. H. & Rupprecht, G. Normal Modes in Hexagonal Boron Nitride. *PhRv* **146**, 543-547 (1966).
16 Nemanich, R. J., Solin, S. A. & Martin, R. M. Light scattering study of boron nitride microcrystals. *Physical Review B* **23**, 6348 (1981).
17 Geick, R., Perry, C. H. & Rupprecht, G. Normal modes in hexagonal boron nitride. *Physical Review B* **146**, 543 (1966).
18 Serrano, J. *et al.* Vibrational properties of hexagonal boron nitride: Inelastic x-ray scattering and ab initio calculations. *Physical Review Letters* **98**, 095503 (Physical Review Letters).